

## The Effects of Attenuation and Site on the Spectra of Microearthquakes in the Shillong Region of Northeast India

RAJIB BISWAS,<sup>1</sup> SANTANU BARUAH,<sup>2</sup> DIPOK K. BORA,<sup>3</sup> ADITYA KALITA,<sup>2</sup> and SAURABH BARUAH<sup>2</sup>

**Abstract**—Microearthquake spectra from the Shillong region are analyzed to observe the effect of attenuation and site on these spectra. The spectral ratio method is utilized to estimate the  $Q$  values for both P- and S-waves in the subsurface layer, wherein the ratio of spectral amplitudes at lower and higher frequencies are taken into consideration for three stations at varying epicentral distances. Average estimates of  $Q_P$  and  $Q_S$  are 178 and 195. The ratio of  $Q_S$  to  $Q_P$  is estimated to be greater than 1 in major parts of the Shillong area, which can be related to the dry crust prevailing in the Shillong region. Typically, the variation in corner frequencies for these spectra is inferred to be characteristic of the site. Simultaneously, observations from spectral content of local earthquakes recorded at two different stations with respect to the reference site yield greater amplification of incoming seismic signals in the frequency range of 2–5 Hz, which is found to be well supported by the existing local lithology pertinent to that region.

**Key words:** Attenuation, site effect, spectra, subsurface.

### 1. Introduction

A seismogram is considered as the convolution of three parameters, namely, source, site and path of propagation up to the receiver station. Usually, seismograms abundant in high-frequency components are more complex to analyze. This is attributed to the fact that these seismograms are endowed with other reflected and refracted phases in addition to the fundamental direct P and S phases. Generally, the S-coda wave trains contribute well to the estimation of some of the fundamental properties, such as attenuation.

Attenuation is defined as the diminution of amplitude of seismic waves during passage from source to receiver site due to energy dissipation (LAY and WALLACE 1995). Generally, the amplitude of the direct seismic wave decays exponentially with increased travel distance (SATO 1977). The decay rates vary inversely as  $Q$ , the quality factor that characterizes attenuation (FRANKEL 1982). According to SATO (1977), high-frequency contents of direct waves help in the determination of the attenuation parameter. The significance of the detailed knowledge of the attenuation mechanism is embedded in the following reasons.

- (a) Measurements of  $Q$  constitute a fundamental tool for the evaluation of the physical states of the rocks (DE LORENZO 1998; ZUCCA *et al.* 1994; SANDERS and NIXON 1995).
- (b) Measurements of  $Q$  are important indicators of macroscale heterogeneities, not only amenable to study the seismic velocities but also to correlate tectonic and near-surface soil and sediments (AKI 1988).
- (c) Detailed knowledge of the path effects due to attenuation is required when correcting the displacement spectra to estimate source parameters of tectonic earthquakes (ABBERCROMBIE and LEARY 1993; ABBERCROMBIE 1995, 1997; SONLEY *et al.* 2006; PREJEAN *et al.* 2001; PRIETO *et al.* 2007).

Many researchers made extensive studies concerning  $Q_P$  and  $Q_S$  for different type of rock formations. Among them, VASSILOU *et al.* (1982) observed that  $Q_P$  equals  $Q_S$  for dry rocks,  $Q_P > Q_S$  for fully saturated rocks, and  $Q_P < Q_S$  for partial saturation. The different heterogeneities in the

<sup>1</sup> Department of Physics, Tezpur University, Tezpur 784028, Assam, India.

<sup>2</sup> Geoscience Division, CSIR North East Institute of Science and Technology, Jorhat 785006, Assam, India. E-mail: saurabhb\_23@yahoo.com

<sup>3</sup> Department of Physics, Diphu Government College, Diphu 782462, Assam, India.

uppermost crust are reported to be the contributing factor towards the disparities observed in  $Q_P/Q_S$ . The presence of heterogeneity in the earth's crust covering a smaller region also helps in estimating the attenuation parameter and, subsequently, the attenuation relation. Additionally, CRANSWICK (1988) and SATO and FEHLER (1998) observed that heterogeneity of the scale of grain sizes plays an important role in the propagation of ultrasonic waves on the order of MHz. The attenuation mechanism in the context of coda  $Q$  was carried out for northeast region of India (NER, India) by HAZARIKA *et al.* (2009). The study reported a relatively smaller attenuation pattern in the Shillong Plateau. While observing seismograms of the earthquakes originating from the city of Shillong and its vicinity, it is found that decay of amplitudes of P- and S-wave trains are quite different from each other, even though similar kind of instrumentation is adopted in the recording stations. The seismograms pertaining to earthquakes, having epicenters in and around Shillong reveal a varying decay rate of S and P wave amplitudes. The seismograms are recorded at three different recording stations, viz; NEHU, SET-UK and IIG which were very close to each other (a spacing of around 7 km or more). All these stations are equipped with identical instrumentations, in order to eliminate different kinds of response spectra, which would be incurred by the adoption of varying sensors and recorders. Despite this, it was observed that the recorded seismograms embody different spectral content, as illustrated in Fig. 1. In that figure, all vertical-component seismograms are displayed which are recorded by the three stations. Figure 1 illustrates an event (all vertical-component seismograms) recorded by the three stations. All three seismograms encompass different spectral content, although the recording stations are very closely spaced. The varying spectral patterns, as observed, necessitate a detailed investigation. In view of this, a straight-forward methodology by FRANKEL (1982), originally developed by TSUJURA (1966), has been followed to ascertain the pattern of attenuation existing in the region. The local site effect at a receiver site that is responsible for enormous scatter is considered while addressing the attenuation.

This manuscript is divided into two parts. In the initial portion, the estimation of attenuation parameters

( $Q$ ) from direct waves is addressed, particularly those of average low- and high-frequency that propagates throughout the near and subsurface of the region under study.  $Q_P$  and  $Q_S$  are computed from the variation of high-frequency energy relative to low-frequency energy pertaining to the local microearthquake activity as a function of travel time/epicentral distance. The attenuation mechanism that is functioning in the region is studied with absolute values of  $Q_P$ ,  $Q_S$  and their ratio. The later part of this work examines the characteristics of the spectra of nearby microearthquakes. This section seeks to study the disparity of the spectral content at the receiving site of the micro-tremors whose incident angle and azimuth are of little variance with respect to the three receiver sites. Additionally, the site amplification patterns pertaining to the three receiving sites are scrutinized, with an attempt to estimate the spectral ratio with respect to a reference site. The spectral ratio with respect to a reference site gives an idea of the site effect in the region, supplemented by litholog information. In this study, the technique adopted by TSUJURA (1966), modified by FRANKEL (1982), has been used to estimate the  $Q_P$  and  $Q_S$  for Shillong. The results of this study are highlighted here.

## 2. Geological Settings

The area of the present study, bounded by latitude 25.40°–26.20°E and longitude 91.40°–92.20°N, encompasses the greater Shillong city region, the capital of Meghalaya, NER, India. It is situated in the Shillong Plateau (SP), covering an area of 6,430 sq. km. It is bounded by the Umiam Gorge to the north, Diengirl Hills to the northwest and Assam Valley to the northeast. The SP, with an Archaean gneissic basement and late Cretaceous–Tertiary sediments along its southern margin, is bounded by the Brahmaputra Graben to the north and by Dauki fault to the south (NANDY 2001).

Shillong forms the type area of the Shillong series of parametamorphites, which includes mostly quartzites and sandstones followed by schist, phyllites, slates etc. The arenaceous phyllites and quartzites are characterized by high resistivities, and the phyllites and metabasic rocks are characterized by

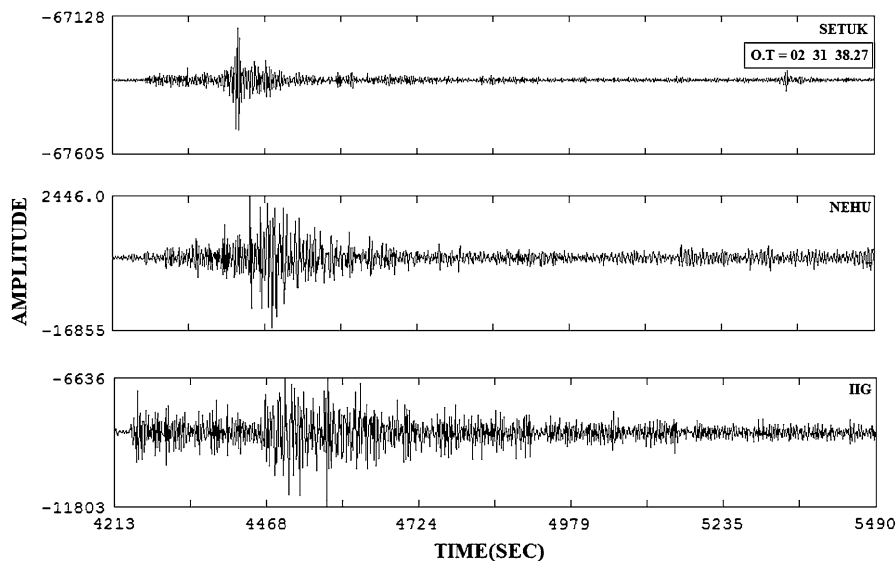


Figure 1

Vertical component seismogram of an event dated 30 March 2009 (no. 11 as enlisted in Table 2), recorded by all the three stations. Origin time and station-code are indicated at the top right corners

high magnetic values, but the magnetic intensities of weathered metabasic rocks and phyllites are comparatively less (PRAKASH *et al.* 1996). The base of the Shillong series of rocks is marked by a conglomerate bed (DEVI *et al.* 2010) containing cobbles and boulders of earlier rocks, i.e., Archaean crystalline, which formed the basement over which the Shillong series of rocks were originally laid down as sedimentary deposits in Precambrian times, probably in shallow marine conditions (RAO *et al.* 2008, 2009). Metasediments and metavolcanic rock associations are the main components of the Shillong basin of Mesoproterozoic period (MITRA 1998), and lithostratigraphically they belong to Shillong Group (Shillong Series of MEDLICOTT 1869) which typified two formations—the Lower Metapelitic Formation (LMF) and the Upper Quartzitic Formation (UQF). The LMF is identified as the Tyrsad Formation (BAROOAH and GOSWAMI 1972), the Barapani Formation (AHMED 1981) and the Manai Formation (BHATTCHARJEE and RAHMAN 1985). The UQF is named the Shillong Formation (BAROOAH and GOSWAMI 1972; AHMED 1981) and the Mawphlang Formation (BHATTCHARJEE and RAHMAN 1985). Metadolerite (erstwhile Khasi greenstone of MEDLICOTT 1869) is found in the form of sills and dykes in both the formations. The rocks of the basin area are

regionally metamorphosed under greenschist facies to the lower part of amphibolite facies (MAZUMDER 1986; DEVI and SARMA 2006). Neoproterozoic granites (e.g., Myllem pluton, Kyrдем pluton and South Khasi pluton) were intruded into the Shillong basin in the form of plutons, which have been dated as  $607 \pm 10$  Ma (CRAWFORD 1969); 885–480 Ma (GHOSH *et al.* 1991, 1994; BHATTACHARYA and RAY BARMAN 1998) and they form another formation namely “Myllem Formation” (GSI 1972). The rocks were intruded by epidiorite rocks, known as “Khasi Greenstone”. The Khasi Greenstone is a group of basic intrusives in the form of linear to curvilinear occurring as concordant and discordant bodies within the Shillong group of rocks and suffered metamorphism (SAR 1973; SRINIVASAN *et al.* 1996). The rocks are widely weathered, and the degree of weathering is found to be more in topographic depressions in comparison to other areas. The metabasic rocks are more prone to weathering than the quartzite rocks (KALITA 1998). In low-lying areas, valley-fill sediments are also prominent. Numerous lineaments of varying magnitude and having major trends in NE–SW, N–S and E–W directions (CHATTOPADHAYA and HASMI 1984; BIDYANANDA *et al.* 2007) are found in the vicinity of Shillong City. The city of Shillong is also marked by undulating terrain.

The area of greater Shillong is part of the Shillong Plateau. The Shillong Plateau is regarded as one of the most seismically active regions in NE India (KAYAL 1987; KAYAL 2008; KAYAL and DE 1987). It is separated out from the peninsular shield and moved to the east by about 300 km along the Dauki fault (EVANS 1964). The study area is juxtaposed between two active faults, i.e., Dhuburi fault and Oldham fault (OLDHAM 1899). It is surrounded by many small and large faults and lineaments. Towards the western part of Shillong, there exists the active Barapani Shear Zone as portrayed in Fig. 2. It is one of the major thrust faults prevailing in this region. The complex geodynamics of the Shillong Plateau resulted in the Great Assam earthquake of 1897. As reported in BILHAM *et al.* (2001), this ( $M_S = 8.7$ ) earthquake caused severe damage to the settlements of this area (Shillong), causing extensive casualties. Mention may be made of the significant earthquake of 1 June 1969 with a magnitude of 5.0, having an epicentral distance of 20 km from Shillong (GUPTA *et al.* 1980). According to Gupta, since 1970 there has been a gradual decrease in P wave velocity, yielding a speculation that the region is experiencing a dilatancy stress precursory to a large earthquake. According to KHATRI *et al.* (1992); the Shillong Massif shows pertinent seismic activity with an average of 10–15 small magnitude earthquakes per day. Over the past 100 years, there were instrumental records of 20 large earthquakes. With the advent of seismic networks set up by NEIST-J (formerly RRL-J) Network, IMD, there has been a tremendous improvement in the micro-tremor records. During the most recent months, there has been a contemporary rise in the number of felt tremors whose epicenters lie within the vicinity of the city of Shillong. This populous city of Shillong is approximately 60 km away from the rupture area of the Great Earthquake of 12 June 1897 ( $M_S = 8.7$ ). The maximum magnitude for historical seismicity has been reported as 8.7 (The Great Shillong Earthquake), whilst for instrumentally recorded seismic activities, the maximum magnitude is 6.2. The moderate magnitude seismicity in the Shillong area is somewhat confined to Barapani Shear zone. All these major tectonic features are portrayed in Fig. 2.

### 3. Data

Since the study relates to the attenuation characteristics and the site effect of microearthquakes in Shillong, earthquake waveforms exclusively from Shillong city and its vicinity are the prime requirement. With this requirement and considering the local geological site condition, a temporary network comprising three stations are installed almost encircling the city. These stations are namely IIG, NEHU and SETUK, as shown in Fig. 3. These were operational during March–April 2009. While designing the instrumentation of this three-station network, the same type of seismograph was used so that frequency characteristics of the system remained unchanged. These stations were equipped with three Trillium 120P seismometers, having a frequency bandwidth of 0.003–50 Hz, with a 24-bit Guralp Digitizer synchronized with a Guralp GPS. Recording in all three stations was continuous. The signals were sampled at 100 samples/s. A total of 135 tremors were recorded during the period of deployment of this temporary network. Out of this, a total of 40 tremors recorded by the three stations were precisely located with the available phase data from the nearby permanent stations. Tables 1 and 2 illustrate the locations of the three nearby stations and hypocentral parameters of the located events, along with epicentral plot as in Fig. 3. Out of these 40 events, only 14 events having epicentral distance of less than 50 km are selected for this study. The depths of the events vary from 4 to 25 km, while the epicentral distance ranges from 1.9 km to 48 km. The root mean square values of the located events is less than 0.2 s. The velocity model of BHATTACHARYA *et al.* (2005) has been utilized with a view to determine the hypocentral parameters. Towards precise location of the events, the Hypocenter Program (LIENERT *et al.* 1986) is used.

The study primarily picks the initial portions of the P and S wave arrivals of the microearthquakes that are utilized to determine the spectra of the P and S waves. Since the events are nearby, with small S–P differences, emphasis has been given to utilizing smaller lengths in order to avoid contamination of the P-portion of the wave with the S wave portion. This is then followed by the baseline correction and trendline removal. In order to calculate the baseline, the

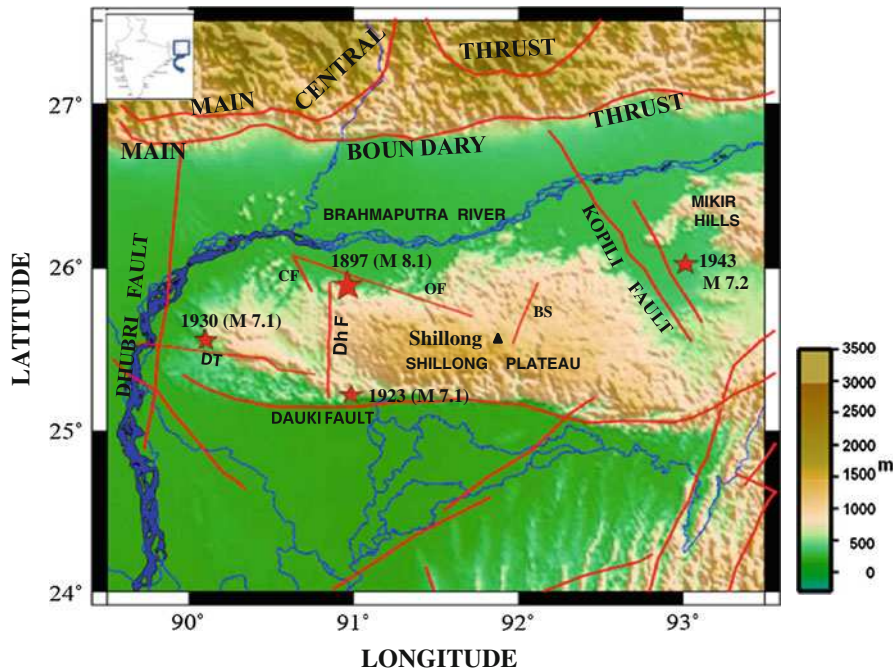


Figure 2

Tectonic settings around Shillong Plateau. The major tectonic features in the region are indicated; *MCT* main central thrust, *MBT* main boundary thrust, *DF* Dauki fault, *DT* Dapsi thrust, *DhF* Dudhnoi fault, *OF* Oldham fault, *CF* Chedrang fault, *BS* Barapani shear zone, *KF* Kopili fault. The great and large earthquakes are shown by red stars. Inset map of India indicating the study region. Color bar represents elevation. The Shillong city is denoted by the triangle. Great and major earthquakes originating in and around Shillong Plateau are indicated by the star symbols, with varying sizes (Inset map of India)

first 128 samples are considered. The trend is subtracted from the original record. Subsequently, the spectra are evaluated using fast-Fourier transform and are subjected to instrumental correction. Towards estimation of the fast-Fourier transform of spectrum, a Matlab code is developed incorporating the desired sample length.

#### 4. Estimation of $Q_P$ and $Q_S$

Generally, events having smaller epicentral distances from recording stations are characterized by seismograms richer in high-frequencies compared to distant events whose epicenter is situated further from the receiving site (BOORE 1983). This fact actually facilitates determination of the coefficient of attenuation from the variations of spectral shapes of the waveforms of the nearby event from a fixed receiver. Figure 4a, b illustrates initial portion of the P-wave and its corresponding displacement spectra at station

IIG for two different earthquakes at nearest and farthest distances, respectively. The spectra are determined for the first 1.28 s of the P-waves of the events. Travel time of the P-wave of the nearest event is 2.11 s, while the distant event has a travel time of 8.87 s. The nearer event is marked by reasonably higher spectral amplitude than that obtained from the distant event as viewed from the logarithmic amplitude scale along Y-axis. Particularly for these two earthquakes, the spectral content shows variation in amplitude from 2 Hz to approximately 11 Hz. At a frequency of 13 Hz and beyond, there is a sharp fall in amplitude. Spectral amplitude in lower frequency range seems to vary between 1 and 3 Hz while for higher frequency range, the variation is observed to be in the range of 9–13 Hz in most of the events. Hence, the variations in spectral amplitudes are anticipated by 2–11 Hz.

Towards determination of  $Q$ , two basic assumptions are made. In most of the cases,  $Q$  is constant over the frequency band studied, 2–11 Hz. In the case

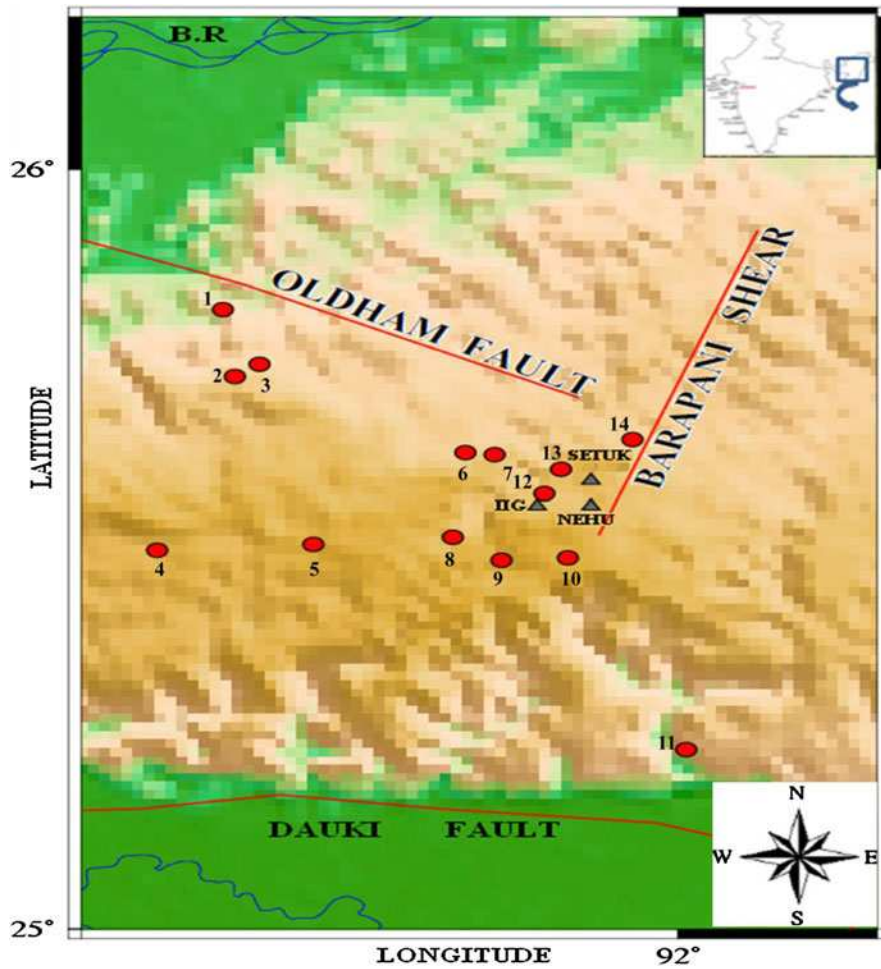


Figure 3

Epicenters used for this study indicated by the *filled circles*. The *triangles* represent the stations temporarily deployed in Shillong city. The *numbers* represents the event numbers as enlisted in the Table 1

Table 1

*Locations of the three stations in Shillong city*

Station name	Latitude (°)	Longitude (°)
IIG	25.558	91.858
SETUK	25.592	91.913
NEHU	25.558	91.911

that  $Q$  varies over this band, then the estimated values of  $Q$  in this work would represent a complicated average of actual  $Q$  values. The second assumption is that the source spectra of all the earthquakes in this study have the same values for the ratio of their 11/2 Hz amplitudes. The ratio of the spectral amplitude at 2 and 11 Hz has been observed for a number

of earthquakes at different epicentral distances from all the earthquakes.

We followed the methodology of TSUJIURA (1966). Spectral amplitude of a body wave at frequency  $f$ ,  $A(f)$  is related to the travel time of the seismic wave  $t$ , the source to receiver distance  $r$ , the spectral amplitude of the source  $A_0(f)$ , the response function of the site  $R(f)$  and  $Q$  by

$$A(f) \propto \left[ \frac{A_0(t)R(f)e^{-\pi ft/Q}}{r} \right]. \quad (1)$$

Now, if there are two frequencies  $f_1$  and  $f_2$ , then the logarithm of the ratio of the spectral amplitudes assumes the form,

Table 2

List of the located hypocentral parameters

Event number	Date			Origin			Latitude (°)	Longitude (°)	Depth (km)	Mag
	yy	mm	dd	hh	mm	ss				
1	09	03	09	15	33	45.39	25.816	91.542	21.81	2.38
2	09	03	09	18	37	49.45	25.728	91.554	30.24	2.60
3	09	03	09	18	36	34.64	25.744	91.579	32.87	2.26
4	09	03	28	09	05	06.80	25.500	91.476	21.67	2.51
5	09	03	29	17	03	08.63	25.508	91.633	20.80	2.39
6	09	03	30	07	31	28.26	25.628	91.786	21.00	1.44
7	09	03	27	35	02	35.41	25.625	91.815	04.09	1.64
8	09	03	31	21	26	16.86	25.517	91.773	20.80	1.87
9	09	03	31	10	15	38.23	25.487	91.822	19.55	2.05
10	09	03	19	17	45	12.73	25.237	92.008	35.04	2.48
11	09	03	30	02	31	38.27	25.490	91.889	18.60	2.17
12	09	03	20	21	03	32.47	25.574	91.865	20.00	1.85
13	09	03	30	19	55	05.92	25.606	91.882	13.30	1.55
14	09	03	22	19	28	57.65	25.645	91.954	09.53	1.62

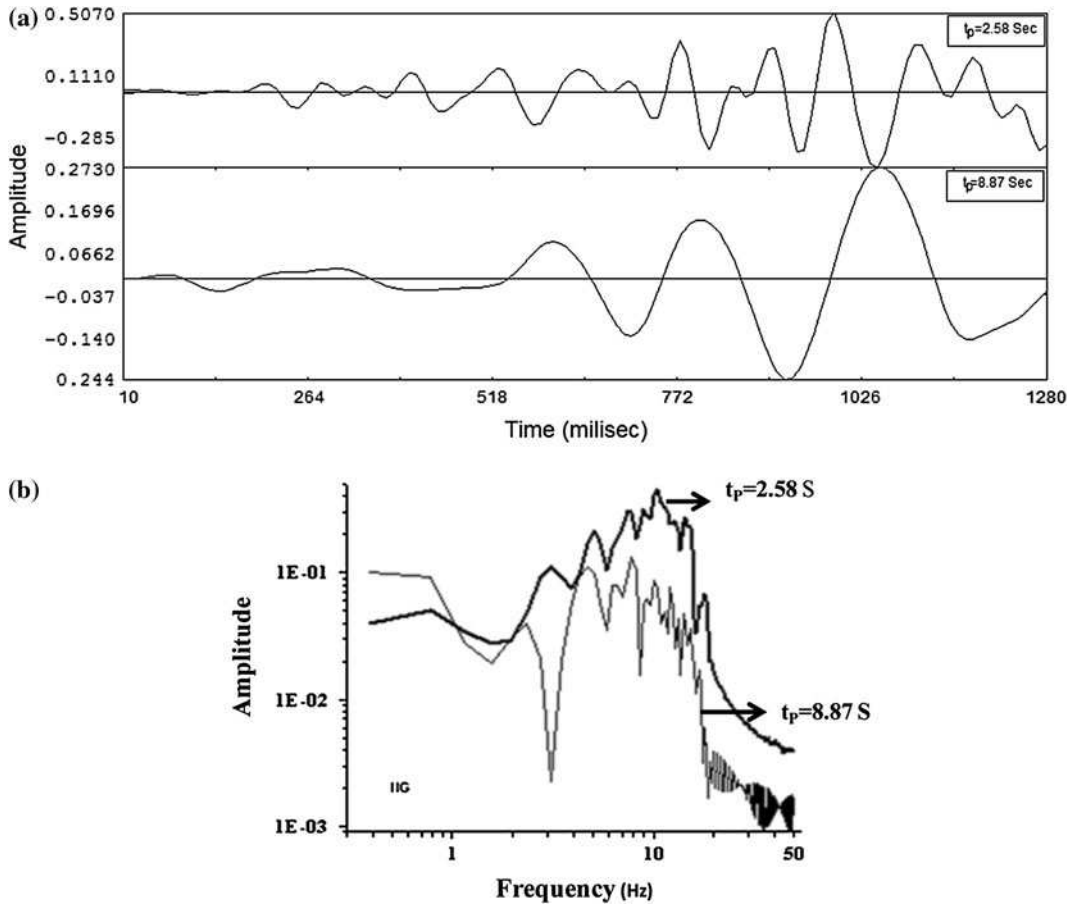


Figure 4

**a** P-waves of closest event with respect to the IIG site, along with the farthest event, **b** displacement spectra of the nearby event with respect to the farthest event recorded at temporary installation IIG, Shillong, NER, India

$$\ln \frac{A(f_1)}{A(f_2)} = \ln \frac{A_0(f_1)}{A_0(f_2)} + \ln \frac{R(f_1)}{R(f_2)} - \frac{\pi(f_1 - f_2)t}{Q}. \quad (2)$$

Considering  $A_0(f_1)/A_0(f_2)$  and  $R(f_1)/R(f_2)$  to be independent of travel time for all the events used in this study, then  $\ln[A_0(f_1)/A_0(f_2)]$  plotted against  $t$  will have a slope of  $\pi(f_2 - f_1)/Q$ . In this work,  $f_1$  and  $f_2$  are chosen to be 11 and 2 Hz, respectively.  $R(f_1)/R(f_2)$  is constant as long as the same station is used in order to determine the amplitude ratios. Additionally, it is also not considered as a function of azimuth or angle of incidence (FRANKEL 1982; BARUAH *et al.* 2007).

$Q_P$  and  $Q_S$  are determined for the events listed in Table 2. P-wave spectra are computed from vertical seismograms. The spectral amplitude ratios of the P-waves for these events are plotted as a function of P-wave travel time ( $t_p$ ) at station IIG. Figure 5a indicates that logarithmic ratio of 11/2 Hz has decreased consistently with the travel time for those events having P-wave travel time greater than 2.2 s. Because of this, events having travel time greater than 2.2 s are taken into consideration, and finally our procedure has yielded a  $Q_P$  of 350 for IIG.

Likewise, S-wave spectra are determined using the horizontal component seismograms. The plot of amplitude ratios of S-waves versus  $t_s$  is displayed in Fig. 6a. Similarly as in Fig. 5a, a constant decay of the ratio of spectral amplitudes with  $t_s$  is observed. The  $Q_P$  and  $Q_S$  values of IIG typically indicate that they are not identical for different paths. Differences in P- and S-wave spectra are estimated from the intercept of regression line. When the differences of amplitude ratios extrapolated to zero travel time, the variations of the spectra at the source characteristics are revealed.

Similarly the spectral ratios of both P- and S-waves for the events recorded at station NEHU are studied as a function of travel time. Incidentally, from Figs. 5b and 6b, it is observed that the spectral ratio of both P- and S-waves at this particular station has decreased approximately at around 2.5 s of travel time. The NEHU data yields a  $Q_P$  of 89 and a  $Q_S$  of 195 from the ratio for 14 numbers of events. The logarithm of the Y-intercept for the P-wave amplitude ratio at zero travel time is observed as 1.9, while the logarithm of the S-wave amplitude ratio at zero travel time is found as 1.6. This small variation in

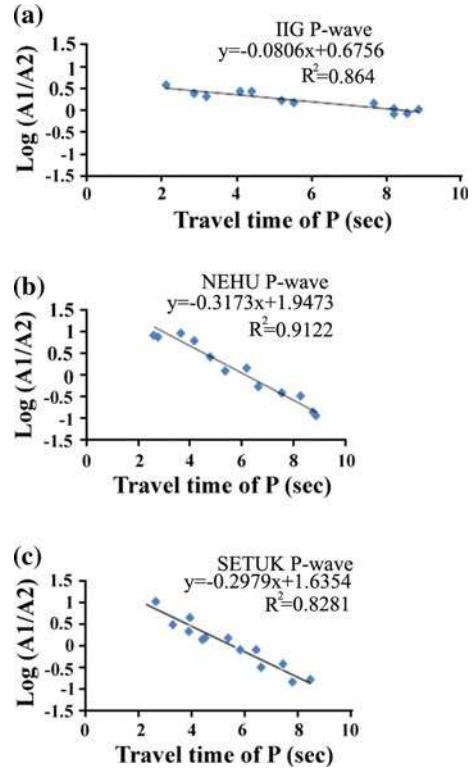


Figure 5

**a** Log of 11 Hz amplitude/2 Hz amplitude plotted against travel time ( $t_s$ ) of each earthquake for P-waves at IIG. The *line* drawn through the data represents the best fit for events with travel time greater than 2 s. **b** Same as in **a** using P-wave spectra at NEHU. The *line* drawn through the data represents the best fit for events with travel time greater than 2.7 s. **c** Same as in **a** but using P-wave spectra at SETUK. The *line* drawn through the data represents the best fit for events with travel time greater than 2.1 s

Y-intercepts between the P- and S-wave data signifies that the frequency content between P- and S-waves of similar travel times was a result of source effects only, not the path effects (FRANKEL 1982). Figures 5c and 6c show the slope of amplitude ratio which allows the estimate of  $Q_P$  as 95 and  $Q_S$  at 225 for the station SETUK.  $Q_P$  and  $Q_S$  values as estimated are given in Table 3. The average estimate of  $Q_P$  and  $Q_S$  from these three particular stations were found to be 178 and 194 respectively.

### 5. Site Effect and Corner Frequency

Although, the epicenters are located very near to the stations, it is implicit that the effect of crustal

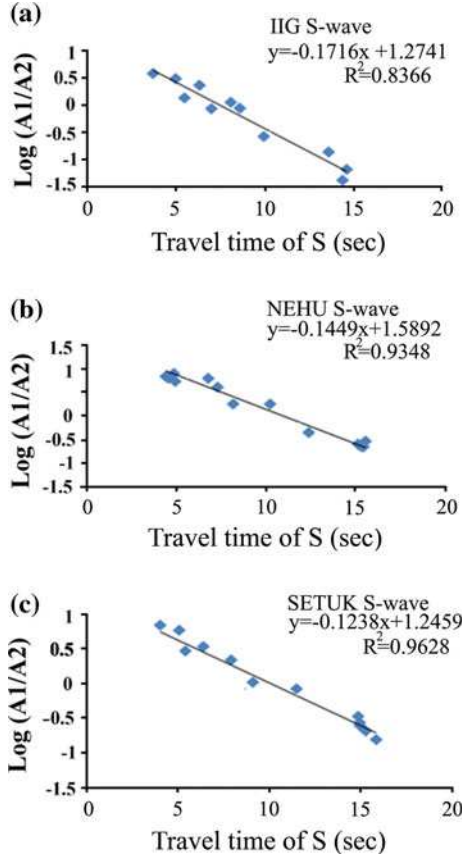


Figure 6

**a** Log of 11-Hz amplitude/2-Hz amplitude plotted against travel time ( $t_s$ ) of each earthquake for S-wave at IIG. The *line* drawn through the data represents the best fit for events with travel time greater than 3.6 s. **b** Same as in **a** using S-wave spectra at NEHU. The *line* drawn through the data represents the best fit for events with travel time greater than 4.4 s. **c** Same as in **a** but using S-wave spectra at SETUK. The *line* drawn through the data represents the best fit for events with travel time greater than 4.0 s

Table 3

Estimated values of  $Q_P$  and  $Q_S$

Quality factors	IIG	NEHU	SETUK
$Q_P$	350	89	95
$Q_S$	164	195	225

attenuation is relatively small. However, effects of site are observed from the spectra of the same event at least for two different stations. The importance of site effect could be observed through inspection of spectra recorded at two different stations of the same event. It was mentioned that similar kinds of instrumentation is

installed in all the stations. Despite this fact, we observe non-uniformity in the spectra. Corner frequencies as observed from P-wave spectra at these two sites appears to be the characteristic of the sites. A corner frequency 15.5 Hz is estimated from the P-wave spectra in SETUK for the event 091533, as listed in Table 2. Similarly, for NEHU, the P-wave spectra of the same event exhibit a corner frequency of 18.5 Hz, as exemplified in Fig. 7. The corner frequencies for these two stations for their respective spectra are estimated for all the events and are listed in Table 4. It is evident from the table that the corner frequencies estimated for SETUK station are found to be higher in most cases, as compared to the NEHU station. These two stations are close together, and the events used for the computation of corner frequencies are within a very small epicentral range of 2–50 km. It is noteworthy that the estimated P-wave corner frequencies for these two stations are higher than the S-wave corner frequencies in all the cases, following the trend as observed by RAUTIAN *et al.* (1978), THATCHER *et al.* (1973) and many others. Even the event 312126 listed in Table 4, with the smallest epicentral distance (2 km from NEHU and 3.5 km from SETUK), shows a dissimilarity of factor three in the estimated values of corner frequencies for the two receiver sites NEHU and SETUK for P-wave spectra. As in the other cases, the S-wave spectra are a bit higher. Keeping in mind the short epicentral distances of these events, the variation in corner frequencies estimated from the spectra of the events recorded by these two stations implies a clear influence of site effect overshadowing the impact of attenuation for this short crustal path. The origin of these observed frequencies are assigned to the properties of the receiver site and not the earthquake sources. Notably, the errors related to the P-wave and S-wave corner frequencies are estimated to be  $\pm 2$  and  $\pm 1$  Hz, respectively. Estimated errors are observed to be larger for P-wave corner frequencies because the higher frequencies are compressed on the logarithmic scale.

### 6. Spectral Content

An attempt has been made to study the disparity of the spectral content as observed in the records of local events when the epicentral distance and the

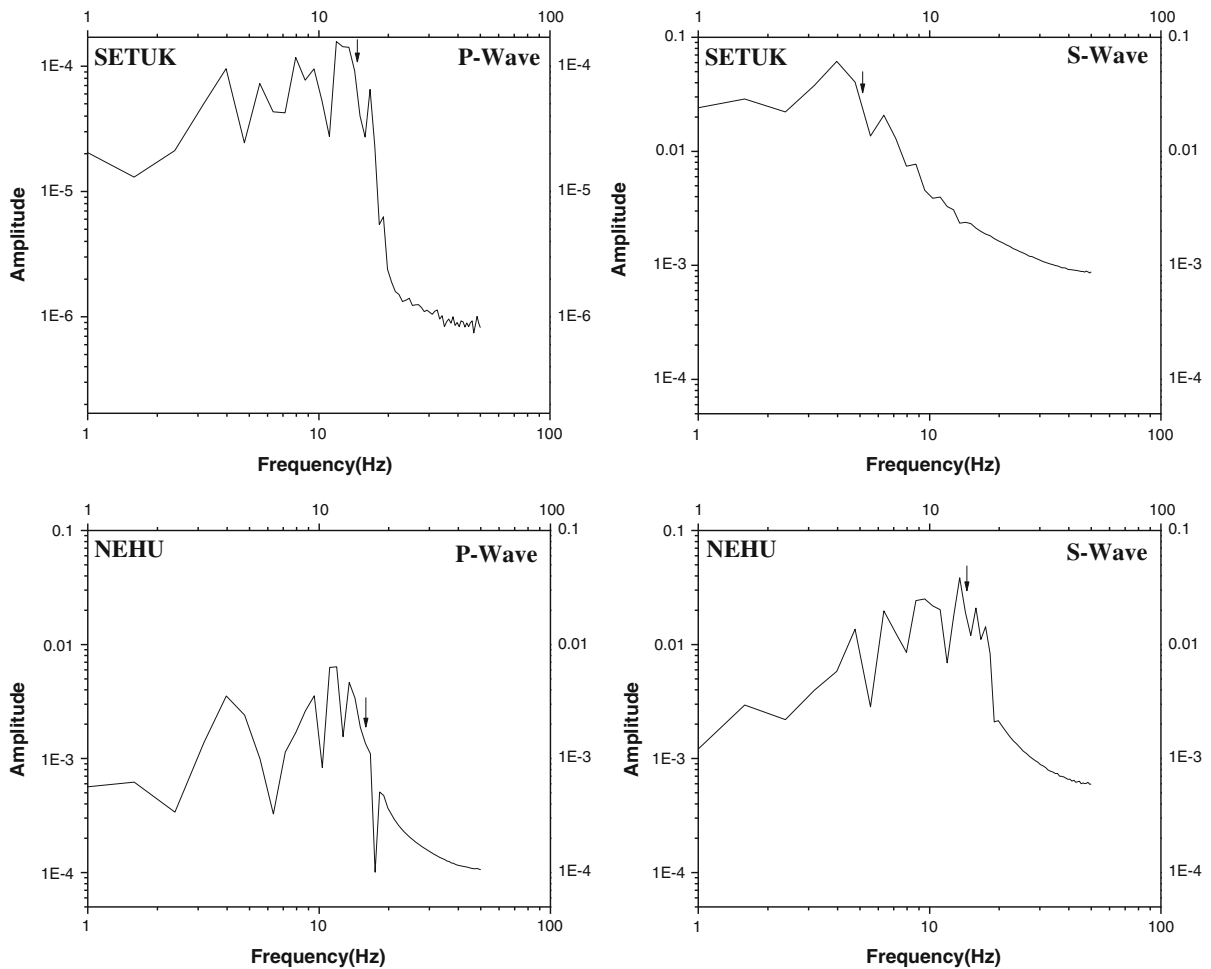


Figure 7

Comparison of P-wave and S-wave displacement spectra of the event listed in Table 2 at SETUK and NEHU. Note that the corner frequency for P-wave is higher at NEHU than SETUK. The respective corner frequencies are indicated by arrow marks

incident angle are practically the same for all the three stations. First, we select and designate the station IIG as hard rock site, and it is considered as the reference station, following STEIDL *et al.* (1996). The spectral ratios are calculated with respect to this particular station. Whole waveform is smoothed by linear regression to restrain some redundant signal existing in the raw waveform, which in particular create 'artificial' enlargement of the spectral ratio. Event numbers 6, 7, 8, 9, 10, 11, 12, 13 and 14 listed in Table 2 are used to observe spectral content, as also illustrated in Fig. 8. Emphasis is given to these nine numbers of events because of their higher signal-to-noise ratios. Only vertical component records are used. Average spectral ratios for SETUK/IIG and

NEHU/IIG are shown in Fig. 9, out of the nine spectral ratios for each case. The average spectral ratios so obtained are found to be more or less stable. It is observed that the spectral ratio does not exhibit large variation within the entire band of frequencies whatever peak amplitude is found; it is delimited within a very narrow spectrum, hinting at moderate dispersion of spectral amplitude. Comparison of the average spectral ratio of NEHU/IIG (red line) and SETUK/IIG (black line) can be seen in Fig. 9a. Fluctuation of the average spectral ratio is observed in the band of 2–6 Hz. The variation of average spectral ratio lies between 0.2 and 7 Hz for NEHU/IIG, i.e., not quite in the same band of oscillations of the average spectral ratio for SETUK/IIG. However,

Table 4

*Estimated corner frequencies for station NEHU and SETUK*

Date						Corner frequency P-wave spectra		Corner frequency S-wave spectra	
yy	mm	dd	hh	mm	ss	NEHU (in Hz)	SETUK (in Hz)	NEHU (in Hz)	SETUK (in Hz)
09	03	09	15	33		45.39	19	16	13
09	03	09	18	37		49.45	19	20	10
09	03	09	18	36		34.64	17	19	08
09	03	19	17	45		12.73	21	20	12
09	03	20	21	03		32.47	16	19	09
09	03	22	19	28		57.65	17	17	10
09	03	27	35	02		35.41	18.5	20	11
09	03	28	09	05		06.80	19	19	09
09	03	29	17	03		08.63	15	17	08
09	03	30	02	31		38.27	21.5	23	13
09	03	30	07	31		28.26	19	20	11
09	03	30	19	55		05.92	20	23	12
09	03	31	10	15		38.23	18	21	10
09	03	31	21	26		16.86	19	22	11

on the contrary, the average spectral ratio for SETUK/IIG in Fig. 9a exhibits strong amplification (maximum of 12) at a frequency around 2.2 Hz. The strong amplification at this frequency reflects the fact that the underlying material beneath the recording site must possess a shear wave velocity gradient. Existence of stronger impedance contrast could be another contributing factor. From this it can be inferred that the geological structures of the north-west part of the Shillong area amplifies about six

times the incoming seismic signal, as compared with the southern part. This effect can be observed at 2–5 Hz only. Variation beyond 5 Hz up to 10 Hz shows site-specific characteristics in the northern and southern parts of the study region.

Generally, directivity plays a very important role in the amplification of phase arrivals, which arises as a result of azimuthal dependence of source time functions of earthquakes due to fault propagation (LAY and WALLACE 1995). Since we have taken into account events from different azimuths, the observed amplification should be primarily considered as a consequence of site geology, nullifying the directivity influence. While correlating the amplification behavior observed in these two sites with available litholog information, there seemed to be a well-defined conformity between these two. As shown in Fig. 9b, the receiver site SETUK is characterized by weathered strata of rocks underlying the soil layer, whilst the other receiver station NEHU is marked by the presence of quartzite rock strata just beneath the soil layer. Since density plays an important role in amplification, weathered formation of rock layers gives rise to higher amplification because of its lower density as compared to quartz formations. This site geology underneath the NEHU station actually supports the relatively smaller amplification compared to SETUK, showing a higher amplification in the same band of frequencies as shown in Fig. 9a.

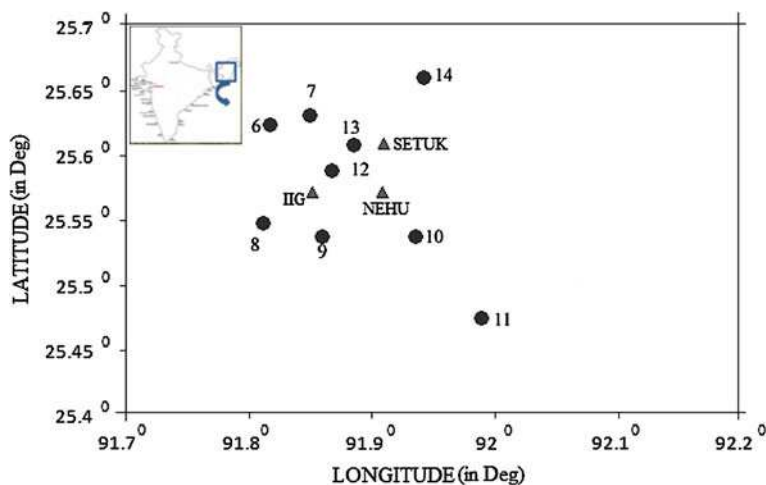


Figure 8

Events utilised in the study of spectral ratio technique with respect to the reference site. *Filled triangles* indicate the location of the seismic sites. The events are shown by *circles*

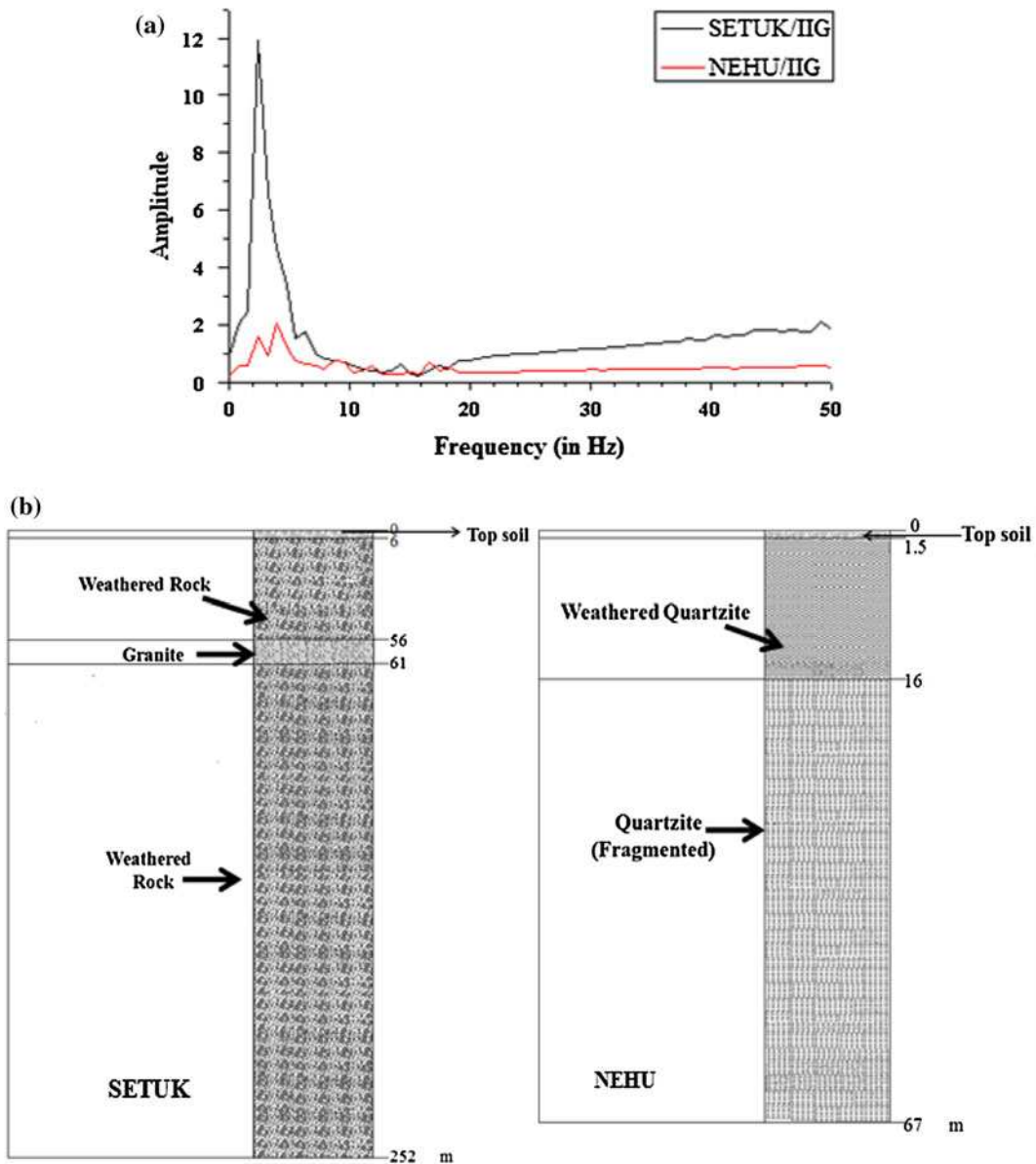


Figure 9

**a** Spectral ratios of two other receiver sites with respect to reference site. Here, IIG is considered as the reference site. **b** The litholog profile of the two stations SETUK and NEHU given by the vertical columns with different legends are redrawn from available borehole information

### 7. Discussion

In this study, we analyze the spectra of the local earthquake events so as to estimate  $Q_P$  and  $Q_S$  on the basis of computations of amplitude of spectral content, site induced corner frequencies and travel time. The objective behind these estimations was to document the influence of the site effect. Various attenuation mechanisms which operate in the earth

may be constrained by the ratio of  $Q_P$ ,  $Q_S$ . ANDERSON *et al.* (1965) observed, from surface wave data,  $Q_P = 9/4 Q_S$  for the asthenosphere, which implicates negligible losses in pure compression. As suggested by AKI (1980), the attenuation of high-frequency S-waves in the lithosphere is incurred by scattering of seismic energy by heterogeneities. If the apparent  $Q$  observed in this study is primarily caused by scattering, the near equivalence of  $Q_P$  and  $Q_S$  has

implications for the size distribution of scatterers in the upper lithosphere.

Another possibility is that the  $Q$  determined in this study is primarily caused by anelasticity. Many of the mechanisms proposed for attenuation are highly sensitive to temperature (JACKSON and ANDERSON 1970) and could be operative at different depths in the earth. If the attenuation is caused by anelasticity, the value of  $Q_P/Q_S$  less than unity found in this study implies that energy losses in compression are smaller than losses in shear for seismic waves traveling through the upper 40 km of the earth.

The short duration of each earth tremor used in this study nullified the adoption of the running average of the small windows over larger windows.  $Q_P$  estimated for NEHU and SETUK are relatively low, while station IIG exhibited higher value of  $Q_P$  and  $Q_S$ . While correlating rock type with  $Q$ , average  $Q_P$  and  $Q_S$  values exhibited availability of the hard granitic rock existing in the region. Average  $Q_S$  obtained for NEHU, SETUK and IIG are higher than average  $Q_P$  with  $Q_S \sim 1.1 Q_P$ . RAUTIAN *et al.* (1978), in their observation, found higher values of  $Q_S$  than  $Q_P$  for paths in the Gharm region of Tajikistan, conforming a theoretical relationship  $t_s Q_s \sim t_p Q_p$ . The similarity in our observation with  $Q_S \sim 1.1 Q_P$  may be attributable to the attenuation mechanism involved with crustal path (RAUTIAN *et al.* 1978). The value of  $Q_S/Q_P$  which is found to be greater than unity suggests that most of the Shillong region is encompassed by dry crust. As the stations were established on the basis of local geological site conditions, observed variation of the  $Q_P$  and  $Q_S$  could be influenced by site effect. The magnitudes of the earthquakes used in the study are appreciably small ( $<2.4$ ); hence the inferred attenuation characteristics might not be representative of relatively higher magnitude earthquakes; however, attenuation mechanisms will remain the same. The P-wave corner frequencies for the events at these stations vary between 17 and 25 Hz. The corner frequencies of the source spectra are primarily a function of the receiving site. This also accounts for the non-linearity of the spectra. The P-wave spectra are abundant in higher mode of frequencies, but as far as the decay rate is concerned, the rate is found to be smaller in case of S-wave spectra after exceeding the corner frequency, whereas it is found to be

comparatively large in case of P-wave spectra. Despite the very short epicentral distances, there is an apparent difference between corner frequencies in the P- and S-wave spectra. This could be an implication of varying rupture area. However, the corner frequencies of S-wave spectra for NEHU and SETUK exhibit marginal difference. This observed variation in the estimates of corner frequencies for these two stations can be related to the influence of site effects and local geology. This result does not indicate that corner frequencies observed at every site will be a manifestation of the material at shallow depth beneath the site. Certain site may be relatively transparent to the passage of high-frequency radiation, while others may be opaque for the same. Consequently, corner frequencies of the source spectra of such frequencies would be much lower than the site-induced corner frequencies (HANKS *et al.* 1984).

Several studies have been carried out towards the determination of quality factors using a fewer number of stations. For example, FACCIOLI *et al.* (2002) accomplished site effect studies using three station arrays in Alpine valleys in northern Italy. SOURIAU *et al.* (2007) performed attenuation study in the city of Lourdes, France, utilizing four stations. A few more studies, such as UMINO and HASEGAWA (1984), HASHIDA (1989), SEKIGUCHI (1991), MITCHELL *et al.* (1997), PHILLIPS *et al.* (2000), (2005), TSUMURA *et al.* (2000), FAN and LAY (2002), TAYLOR *et al.* (2003), and XIE *et al.* (2004), are carried out for the purpose of the determination of quality factors using fewer stations. Since only three stations were utilized in this study, the attenuation relation estimated might at best be approximate. There seemed to be a noticeable correlation between the spectral ratio at the frequency range between 0.5 and 5.0 Hz and the near- and subsurface lithology of the area where the recording stations are located. The correlation is visible in the frequency band of 2–5 Hz. Within this bandwidth, the impending signal is amplified six times at the receiver site at station SETUK, compared to the other station at NEHU at a frequency of 2.6 Hz. This might indicate that seismic signals traversing the crustal path leading to these receiver sites, which are located at northeastern part (SETUK) and southwestern (NEHU) part of the Shillong region, undergo different levels of amplification. This may be attributed to

the characteristic soil, supplemented by weathered and fractured zones underneath the site of the stations, which is well substantiated by the available borehole information.

### 8. Conclusion

The evaluation of  $Q_P$  and  $Q_S$  based on the present technique yields the inference that the microearthquakes originating within the Shillong region are characterized by the influence of attenuation as well as site effects. So far, it has been observed that epicentral distance play a major role shaping the spectral content. Non-equivalence in average estimate of  $Q_P$  and  $Q_S$  is observed, however, in most cases the higher values of  $Q_S$  compared to  $Q_P$  signifies the greater penetration of seismic energy. The study suggests that most of the Shillong region is covered by the dry crust, as it is characterized by the ratio of  $Q_P/Q_S$  being larger than unity. Ultimately, the high- $Q$  zone corresponds to the dense and high-velocity rocks of the region. Thus the variation of quality factors for P- and S-waves at different stations builds an estimate of site-specific anelastic responses of the seismic source and the respective paths. Additionally, the varying corner frequencies in cases of both P- and S-wave spectra at all the three stations seem to be characterized by site effects, even though the receiving sites are in a close neighborhood. Finally, the spectral ratio gives the inference that the north-eastern part of the Shillong region amplifies six times the incoming signal as compared to the south-western part, probably due to the existence of a weathered zone underneath. The attenuation relations for quality factors obtained here may be used for the estimation of source parameters and the near-source simulation of earthquake ground motion of the earthquakes, which in turn are required for the assessment of seismic hazard in the region.

### Acknowledgments

We express our sincere gratitude to Dr. P.G. Rao, Director, NEIST-Jorhat for his constant encouragement and permission to publish the work. We are also

grateful to MoES, New Delhi for their financial support vide sanction number MoES/23(533)/SU/2005. At the same time, we extend our gratitude to the two anonymous reviewers for their constructive criticism.

### REFERENCES

- ABBERCROMBIE, R., and LEARY, P. (1993), *Source parameters of small earthquakes recorded at 2.5 km depth Cajon Pass: Southern California: Implications for earthquake scaling*, Geophys. Res. Letters, 20, 1511–1514.
- ABBERCROMBIE, R.E. (1995), *Earthquake source Scaling Relationship from  $-1$  to  $5 M_L$  using seismograms recorded at 2.5 km depth*, J. Geophys. Res. 100, 24, 015–24, 036.
- ABBERCROMBIE, R.E. (1997), *Near Surface attenuation and site effects from comparison of Surface and Boreholes Recordings*. Bull. Seismol. Soc Am. 87, 731–744.
- AHMED, M. (1981) *Stratigraphic Class of Shillong Group, Khasi Hills, Meghalaya*, J. Mines, Metals and Fuels. Sept–Oct., 295–297.
- ANDERSON, D. L., BEN-MENACHEM A., and ARCHAMBEAU C.B. (1965), *Attenuation of seismic energy in the upper mantle*, J. Geophys. Res. 70, 1441–1448.
- AKI, K. (1980), *Attenuation of shear waves in the lithosphere for frequencies from 0.05 to 25 Hz*, Phys. Earth Planet. Int. 21, 50–60.
- AKI, K. (1988). *Local site effects on ground motion, Earthquake Engineering and Soil Dynamics II-Recent Advances in Ground Motion Evaluation*, Proceeding of the A.S.C.E. Speciality Conference, Park City, Utah, June 27–30, 103–155.
- BAROOAH, B.C. and GOSWAMI, I.D. (1972), *Precambrian stratigraphy of the Assam plateau*; J. Mines, Metals and Fuel 20, 368–373.
- BARUAH, S., HAZARIKA, D., GOGOI, N. K., and RAJU P.S. (2007), *The effects of attenuation and site on the spectra of microearthquakes in the Jubille Hill region of Hyderabad, India* J. Earth Sys Sci. 116, 37–47.
- BHATTACHARJEE, C. C and RAHMAN, S. (1985) *Structure and lithostratigraphy of the Shillong Group of rocks of East Khasi Hills of Meghalaya*, Bull. Geol. Min. Met. Soc. India, 53, 90–99.
- BHATTACHARYA, P. M., PUJOL, J., MAZUMDAR, R. K., and KAYAL, J. R. (2005), *Relocation of earthquakes in the Northeast India region using joint Hypocenter determination method*, Curr. Sci. 89(8), 1404–1413.
- BHATTACHARYA, B.P. and RAY BARMAN, T. (1998), *Precambrian geology in Northeastern India: A perception of contribution during Pre and Post Independence Era*; M.S. Krishnan Centenary Commemorative, National Seminar, 12 November 1998, Calcutta, 11–12.
- BIDYANANDA, M., and DEOMURARI, M.P. (2007), *Geochronological constraints on the evolution of Meghalaya massif, northeastern India: An ion microprobe study*. Curr. Sci. 93, 1620–1623.
- BILHAM, R., and ENGLAND, P. (2001), *Plateau pop-up in the Great 1897 Assam earthquake*, Nature, 410, 806–809.
- BOORE, D.M. (1983), *Stochastic simulation of high-frequency ground motions based on seismological models of the radiated spectra*, Bull. Seism. Soc. Am. 73, 1865–1894.

- CHATTOPADHAYA, N., and HASHIMI, S. (1984), *The Sung valley alkaline ultramafic carbonate complex, East Khasi Hills district, Meghalaya*, Rec. Geo. Surv. India 113, 24–33.
- CRANSWICK, E. (1988), *The information content of high frequency seismograms and the near-surface geologic structure of 'hard rock' recording sites*, Pure Appl. Geophys. 128, 333–363.
- CRAWFORD, A.R. (1969), *India, Ceylon and Pakistan: New age data and comparison with Australia*, Nature 223 80–84.
- DE LORENZO, S. (1998), *A Model to Study the Bias on Q Estimates Obtained by applying the Rise Time Method to Earthquake Data*, Pure Appl. Geophys. 153, 419–438.
- DEVI, N.R. and SARMA, K. P. (2006), *Tectonostratigraphic study of conglomerates of Shillong Basin of Meghalaya, India*; J. Geol. Soc. India, 68, 1100–1108.
- DEVI, N and SARMA, K.P. (2010), *Strain analysis and stratigraphic status of Nongkhya, Sumer and Mawmaram conglomerates of Shillong basin, Meghalaya, India*, J. Earth Sys. Sci. 119(2), 2010, 161–174.
- EVANS, P. (1964), *The Tectonic Framework of Assam*, J Geol. Soc. India 5, 80–96.
- FACCIOLI, E., VANINI, M., and FRASSINE, L. (2002), *Complex site effects in earthquake strong motion, including topography*, 12th European Conference on Earthquake Engineering, Soc. Earthquake and Civ. Eng. Dyn., London.
- FAN, G., and LAY, T. (2002), *Characteristics of Lg attenuation in the Tibetan Plateau*, J. Geophys. Res. 107 (B10), 2256, doi: [10.1029/2001JB000804](https://doi.org/10.1029/2001JB000804).
- FRANKEL, A. (1982), *The effects of attenuation and site response on the spectra of micro earthquakes in the Northeastern Caribbean*, Bull. Seism. Soc. Am. 72(4), 1379–1402.
- GHOSH, S., CHAKRAVORTY, S., BHALLA, J. K., PAUL, D.K., SARKAR, A., BISHURI, P. K and GUPTA, S.N. (1991), *Geochronology and geochemistry of granite plutons from East K. Hills, Meghalaya*; J. Geol. Soc. India 37, 331–342.
- GHOSH, S., CHAKRABORTY, S., BHALLA, J. K., PAUL, D. K., SARKAR, A., BISHUI, P. K. and GUPTA, S.N. (1994), *New Rb-Sr isotopic ages and geochemistry of granitoids from Meghalaya and their significance in middle to late Proterozoic crustal evolution*; Ind. Minerals 48(1&2), 33–44.
- GUPTA, H.K., and SINGH, V.P. (1980), *Teleseismic P-wave residual Investigations at Shillong, India*, Tectonophys. 66, 19–27.
- Geological Survey of India (1972) Code of stratigraphic nomenclature of India; Misc. Publ. 20, 28 pp.
- HANKS, T. C., BUCKNAM, R. C, LAJOIE, K. R., and WALLACE, R. E. (1984), *Modification of wave-cut and faulting controlled landforms*. Geophys. Res. 89, 5771–5790.
- HASHIDA, T. (1989), *Three-dimensional seismic attenuation structure beneath the Japanese islands and its tectonic and thermal implications*, Tectonophys. 159, 163–180.
- HAZARIKA, D., and BARUAH, S. (2009), *Attenuation of Coda waves in Shillong and Mikir Hills Plateau, NE India*. J. Seism. 13 (1), 141–160, doi:[10.1007/s10950-008-9132-0](https://doi.org/10.1007/s10950-008-9132-0).
- JACKSON, D. D. and ANDERSON D. L. (1970), *Physical mechanisms of seismic wave attenuation*, Rev. Geophys. Space Phys. 8, 1–63.
- KALITA, B.C. (1998), *Ground water prospects of Shillong Urban Agglomerate*. Unpublished
- KAYAL, J.R. (1987), *Microseismicity and source mechanism study: Shillong Plateau, northeast India*. Bull. Seism. Soc. Am. 77, 184–194.
- KAYAL, J.R. and DE, R. (1987), *Pn velocity study using a temporary seismograph network in the Shillong Plateau, northeast India*. Bull. Seism. Soc. Am. 77, 1718–1727.
- KAYAL, J.R. (2008). *Microearthquake Seismology and Seismotectonics of South Asia*. Springer, pp 273–275.
- KHATRI, K.N., CHANDER, R., MUKHOPADHYAY, S., SRIRAM, V., and KHANAL, K.N. (1992), *A model of active tectonics in the Shillong Massif region, Himalayan Orogen and Global Tectonics*.
- LAY, T. and WALLACE, T. C. (1995), *Modern Global Seismology*. Academic Press, San Diego, CA, pp. 521.
- LIENERT, B. R., BERG, B. E., and FRAZER, L. N. (1986), *Hypocenter: An earthquake location method using centered, scaled and adaptively damped least squares*, Bull. Seism. Soc. Am. 76, 771–783.
- MAZUMDER, S. K. (1986), *The Precambrian framework of part of the Khasi Hills, Meghalaya*, GSI Record. 117(2), 1–59.
- MEDLICOTT, H. B. (1869), *Geological sketch of the Shillong Plateau in North-Eastern Bengal*, Geol. Soc. India Memo. VII (1), 197–207.
- MITCHELL, B. J., PAN, Y., XIE, J and CONG, L. (1997), *Lg coda Q variation across Eurasia and its relation to crustal evolution*, J. Geophys. Res. 102, 22, 767–22, 779.
- MITRA, S. K. (1998) *Polydeformation of rocks of the Shillong Group around Sohiong, Khasi Hills*, Ind. J. Geol. 70(1&2), 123–131.
- NANDY, D.R. (2001), *Geodynamics of Northeastern India and the adjoining region*. ACB publications, Calcutta: pp. 209.
- OLDHAM, R.D. (1899), *Report on the great earthquake of 12th June 1897*. Mem Geol Surv India, 29, 1–379.
- PHILLIPS, W.S., HARTSE, H.E., TAYLOR, S.R. and RANDALL, G.E. (2000), *1 Hz Lg Q tomography in central Asia*, Geophys. Res. Lett. 27, 3425–3428.
- PHILLIPS, W. S., HARTSE, H. E and RUTLEDGE, J. T. (2005), *Amplitude ratio tomography for regional phase Q*, Geophys. Res. Lett. 32.
- PRAKASH, D., ROY J.C. and NAYAK P.N. (1996), *Geophysical investigations for detecting zones of sulphide mineralization in Barapani—Mawing Area, Khasi Hills Meghalaya (NER-1028)*. Memo. Geol. Soc. India.
- PREJEAN, G.S., and ELLSWORTH, W.L. (2001), *Observations of Earthquake Source Parameters at 2 km Depth in the Long Valley Caldera, Eastern California*. Bull. Seism. Soc. Am. 91(2), 165–177.
- PRIETO, G.A., THOMSON, D.J., SHEARER, P.M., and PERKER, R.L. (2007), *Confidence intervals for earthquake source parameters*, 168, 1227–1234.
- RAO, J.M., and RAO, P.G.V.S (2008), *Geology, Geochemistry and Palaeomagnetic study of Cretaceous Mafic Dykes of Shillong Plateau and Their Evolutionary History Indian Dykes: Geochemistry, Geophysics and Geomorphology*, 589–607.
- RAO, J.M., and RAO, G.V.S.P (2009), *Precambrian mafic magmatism of Shillong plateau, Meghalaya and their evolutionary history*. J Geol. Soc. India, 73,143–152.
- RAUTIAN, T. G., KHALTURIN, V. I., MARTINOV, V. G., and MOLNAR, P. (1978), *Preliminary analysis of the spectral content of P and S waves from local earthquakes in the Garm, Tadzhikistan region*, Bull. Seism. Soc. Am. 68, 949–972.
- SANDERS, C. O., and NIXON, L.D. (1995), *S-wave Attenuation Structure in Long Valley Caldera, California, from Three-component S-to-P Amplitude Ratio Data*, J. Geophys. Res. 100, 12, 395–12, 404.
- SAR, S.N. (1973), *An interim report on ground water exploration in the Greater Shillong area, Khasi Hills District, Meghalaya: Memo report*, Central Ground Water Board.

- SATO, H. (1977), *Energy propagation including scattering effects: single isotropic scattering*; J. Phys. Earth. 25, 27–41.
- SATO, H., and FEHLER, M. (1998), *Seismic wave propagation and scattering in the Heterogeneous Earth*, AIP Press/Springer Verlag, New York.
- SEKIGUCHI, I. (1991), *Three-dimensional  $Q$  structure beneath the Kanto-Tokai district, Japan*, Tectonophys. 195, 83–104.
- SONLEY, E., and ABBERCROMBIE, R.E. (2006), *Geophysical Monograph Series*.
- SOURIAU, A., ROULLÉ, A and CHRISTIAN, P. (2007), *Site Effects in the City of Lourdes, France, from H/V Measurements: Implications for Seismic-Risk Evaluation*, Bull. Seism. Soc. Am. 97(6), 2118–2136.
- SRINIVASAN, P., SEN, S., and BANDOPADHAYA, P.C. (1996), *Study of variation of Paleocene-Eocene sediments in the shield areas of Shillong Plateau*. Rec. Geol. Surv. India 129, 77–78.
- STEIDL, J. H., TUMARKIN A.G., and ARCHULETA, R. J. (1996), *What is a reference site?* Bull. Seism. Soc. Am. 86, 1733–1748.
- TAYLOR, S. R., YANG, X., and PHILLIPS, W. S. (2003), *Bayesian  $L_g$  attenuation tomography applied to eastern Asia*, Bull. Seismol. Soc. Am. 93, 795–803.
- THATCHER, W. and HANKS T. C. (1973), *Source parameters of Southern California earthquakes*, J. Geophys. Res. 78, 8547–8576.
- TSUMURA, N., MATSUMOTO, S., HORIUCHI, S. and HASEGAWA, A. (2000), *Three dimensional attenuation structures beneath the northeastern Japan arc estimated from spectra of small earthquakes*, Tectonophys. 319, 241–260.
- TSUJURA, M. (1966), *Frequency analysis of seismic waves, I*, Bull. Earth. Res. Inst., Tokyo Univ. 44, 873–891.
- UMINO, N., and HASEGAWA, A. (1984), *Three-dimensional  $Q_s$  structure in the northeastern Japan arc*, J. Seism. Soc. Japan. 37, 217–228 (in Japanese with English abstract).
- VASSILOU, M, SALVADO, C. A., and TITTMANN, B. R. (1982), *Seismic attenuation*, In: *CRC Handbook of Physical Properties of Rock, III* (ed.) R S Carmichael, CRC press, Boca Raton, Florida.
- XIE, J., GOK, R., NI, J and AOKI, Y. (2004), *Lateral variations of crustal seismic attenuation along the in depth profiles in Tibet from  $L_g$   $Q$  inversion*, J. Geophys. Res. 109.
- ZUCCA, J.J., HUTCHINGS L.J., and KASAMEYER, P.W. (1994), *Seismic Velocity and attenuation structure of the Geysers Geothermal Field, California*. Geothermics, 23, 111–126.

(Received January 5, 2012, revised November 7, 2012, accepted November 27, 2012)